J Physiol 588.3 (2010) pp 447–463

The Journal of Physiology

NMDAR-mediated EPSCs are maintained and accelerate in time course during maturation of mouse and rat auditory brainstem *in vitro*

Joern R. Steinert, Michael Postlethwaite*, Melissa D. Jordan*, Tatyana Chernova, Susan W. Robinson and Ian D. Forsythe

MRC Toxicology Unit, Hodgkin Building, and Dept Cell Physiology & Pharmacology, University of Leicester, Leicester LE1 9HN, UK*

NMDA receptors (NMDARs) mediate a slow EPSC at excitatory glutamatergic synapses throughout the brain. In many areas the magnitude of the NMDAR-mediated EPSC declines with development and is associated with changes in subunit composition, but the mature channel composition is often unknown. We have employed the calyx of Held terminal with its target, the principal neuron of the medial nucleus of the trapezoid body (MNTB), to examine the NMDAR-mediated EPSC during synapse maturation from P10 to P40. Our data show that the calyx has reached a mature state by around P18. The NMDAR-mediated EPSC amplitude (and dominant decay τ) fell from around 5 nA (τ: 40–50 ms) at P10/11 to 0.3–0.5 nA (τ: 10–15 ms) by P18. The mature NMDAR-EPSC showed no sensitivity to ifenprodil, indicating lack of NR2B subunits, and no block by submicromolar concentrations of zinc, consistent with NR1-1b subunit expression. Additionally, from P11 to P18 there was a reduction in voltage-dependent block and the apparent dissociation constant for $[Mg^{2+}]_o$ (K_o) changed from 7.5 to 14 mM. Quantitative PCR showed that the relative expression of NR2A and NR2C increased, while immunohistochemistry confirmed the presence of NR2A, NR2B and NR2C protein. Although the mature NMDAR-EPSC is small, it is well coupled to NO signalling, as indicated by DAR-4M imaging. We conclude that *native* mature NMDAR channels at the calyx of Held have a fast time course and reduced block by $[Mg^{2+}]_o$, consistent with dominance of NR2C subunits and functional exclusion of NR2B subunits. The pharmacology suggests a single channel type and we postulate that the mature NMDARs consist of heterotrimers of NR1-1b–NR2A–NR2C.

(Resubmitted 6 November 2009; accepted after revision 11 December 2009; first published online 14 December 2009)
Corresponding author I. D. Forsythe: MRC Toxicology Unit, Hodgkin Building, University of Leicester, Leicester LE1 9HN, UK. Email: idf@le.ac.uk

Abbreviations: AMPA(R), α-amino-3-hydroxyl-5-methyl-4-isoxazole-propionate (receptor); AP, action potential; D-AP5, D-2-amino-5-phosphonovalerate; GluRDo, glutamate receptor subunit 4 (or D) flop spliced variant; HP, holding potential; Kv3, voltage-gated K^+ channel, third family; MNTB, medial nucleus of the trapezoid body; NMDA(R), *N*-methyl-D-aspartate (receptor); NR1 and NR2, NMDA receptor subunits; qPCR, quantitative real time PCR; RT, room temperature; tPA, tissue plasminogen activator.

Introduction

NMDA receptor (NMDAR) activation by glutamate produces long bursts of channel openings (Gibb & Colquhoun, 1992) which at excitatory synapses generate slow time course voltage-dependent EPSPs with an additional intracellular signal through their permeability to Ca^{2+} ions (together with Na^+ and K^+). The voltage dependence of the EPSP is accomplished with channel block by $[Mg^{2+}]_o$, being relieved on depolarisation from resting membrane potentials, thereby providing a conditional regulator of NMDAR activity (Mayer *et al.* 1984; Nowak *et al.* 1984; Mayer & Westbrook, 1987). NMDARs act in concert with fast time course AMPAR-mediated EPSCs to mediate transmission at excitatory synapses, forming a stereotypical dual component response to the transmitter glutamate (Dale & Roberts, 1985; Forsythe & Westbrook, 1988). Relief of the voltage-dependent block of the NMDAR channel by $[Mg^{2+}]_o$ on depolarization is the basis of coincidence detection, which together with the Ca^{2+} permeability, allows synaptic NMDARs to trigger activity-dependent changes underlying developmental plasticity, learning and memory in many areas of the brain (Aamodt &

DOI: 10.1113/jphysiol.2009.184317

Constantine-Paton, 1999; Bliss *et al.* 2003; Cull-Candy & Leszkiewicz, 2004; Kerchner & Nicoll, 2008).

NMDARs mediate a slow EPSC in both auditory brainstem relay synapses of the endbulb and calyx of Held (Forsythe & Barnes-Davies, 1993; Zhang & Trussell, 1994; Barnes-Davies & Forsythe, 1995; Isaacson & Walmsley, 1996). These relay synapses mediate transmission across the brainstem for binaural comparison of auditory inputs in mechanisms of sound source localization (Oertel, 1999). In young animals (less than postnatal day (P) 11) the NMDAR currents are several nanoamps in amplitude (in the absence of Mg^{2+} block) and clear evidence from several groups shows that their magnitude declines on maturation as the auditory pathway becomes functional on opening of the auditory canal (Taschenberger & von Gersdorff, 2000; Futai *et al.* 2001; Joshi & Wang, 2002), which occurs from around P11 in mice and rats. Accumulation of NMDAR currents at resting membrane potentials during high frequency synaptic trains has been shown in young animals. Extrapolation of such data from young animals and responses measured at room temperature have suggested that the NMDAR-EPSC virtually disappears on maturation, and it is sometimes suggested that NMDARs are redundant at mature brainstem synapses. Due to the technical difficulties of recording in mature brainstem, there are only a few reports of NMDAR-mediated EPSCs from medial nucleus of the trapezoid body (MNTB) neurons in rodents older than 14 days and fewer studies still have measured these currents at physiological temperatures. Our aim here is to fill this knowledge gap by studying NMDR-EPSCs in older animals at physiological temperatures and to use pharmacological tools and immunohistochemistry to identify the putative subunit composition of native NMDARs at the mature calyx of Held synapse.

The calyx of Held is the largest excitatory synapse in the CNS (Held, 1893; Forsythe, 1994; von Gersdorff & Borst, 2002; Schneggenburger & Forsythe, 2006) and is an ideal site to study the properties and composition of synaptic NMDARs. The giant synapse and its target neuron are highly stereotyped, the synapse is located on the cell body, and voltage-clamp can be conducted with good space-clamp. Its large, fast-time-course, AMPAR-mediated EPSC guarantees the firing of a short latency postsynaptic action potential (AP) in the target neuron (the principal neuron of the MNTB) while several voltage-gated potassium channels, particularly Kv1 (Brew & Forsythe, 1995; Klug & Trussell, 2006) and *ether-à-go-go*-related gene (ERG) K^+ channels (Hardman & Forsythe, 2009) suppress multiple AP firing during the decay of each EPSP. Nevertheless, it is clear that the large NMDAR-mediated synaptic conductance can contribute to excitability in young animals (Futai *et al.* 2001), but at the mature calyx where the NMDAR-EPSC is small, the dominant action is the activation of nitric oxide synthase (Steinert *et al.* 2008) rather than electrical signalling.

We have conducted whole-cell patch recordings from synaptically connected MNTB neurones, and employed pharmacology, quantitative real-time PCR (qPCR), immunohistochemistry and nitric oxide imaging to examine NMDAR-mediated responses across an age range from around hearing onset at P11 to weaning at P21 in rats and mice and continuing to as old as P40 in mice (around the age of female sexual maturity). Our results show that NMDAR-mediated EPSCs are faster and larger at physiological temperatures compared to room temperature at any age tested. Although the NMDAR-EPSC amplitude declines over this developmental period, it stabilises at around P18 and is maintained. The properties of the NMDAR-EPSC are consistent with previous reports of a developmental shift from NR2B to NR2A subunits during development. Here we report that there is a further change with synaptic NMDAR showing reduced sensitivity to $[Mg^{2+}]_o$ block from P11 to P18, consistent with incorporation of NR2C subunits at mature brainstem synapses. We conclude that synaptic NMDARs are maintained and are functional in the auditory brainstem of mature animals.

Methods

Preparation of brain slices

Brainstem slices containing the superior olivary complex (SOC) were prepared from Lister Hooded rats or CBA/Ca mice. All procedures were carried out in compliance with the policies and regulations set out by Drummond (2009) and with the guidelines laid down by the University of Leicester animal welfare committee. Animals were killed by decapitation in accordance with the Animals (Scientific Procedures) Act 1986, and brain slices prepared as described previously (Wong *et al.* 2003) using animals between 10 and 40 days old. In brief, transverse slices of the SOC containing the MNTB were cut with varying thickness according to age (in rat, to aid visualisation in the older rats which have more myelination; 220 μm at 10/11 days, 200 μm at 14 days, 180 μm at 18 days and 160 μm at 21 days); slices from mice were all 200 μm thick. This procedure took place in low sodium artificial cerebrospinal fluid (aCSF) at ∼0°C, and slices were then stored at 37°C for 1 h in normal aCSF, after which they were stored at room temperature (∼20°C) until use. Composition of the normal aCSF was (mM): NaCl 125, KCl 2.5, $NaHCO_3$ 26, glucose 10, NaH_2PO_4 1.25, sodium pyruvate 2, *myo*-inositol 3, $CaCl_2$ 2, $MgCl_2$ 1 and ascorbic acid 0.5; pH was 7.4 when continuously bubbled with 95% O_2–5% CO_2. In the low-sodium aCSF, NaCl was replaced by 250 mM sucrose and $CaCl_2$ and $MgCl_2$ concentrations were 0.1 and 4 mM, respectively.

Imaging and electrophysiology

In order to identify neurones with intact synaptic connections, an imaging technique was used as previously described (Billups *et al.* 2002). Briefly, cells were loaded with 7 μM Fura 2 acetoxymethyl ester (Fura 2-AM; Molecular Probes, Eugene, OR, USA) for ∼4–7 min and then viewed with a Photometrics Cool SNAP-fx camera after a single 100 ms exposure to light at 380 nm wavelength (provided by a xenon arc lamp controlled by a Cairn Optoscan monochromater; Cairn Instruments, Faversham, UK). Fluorescence images were displayed using the Metafluor imaging suite software (v. 7, Molecular Devices, Sunnyvale CA, USA). A region of interest was drawn around labelled neurons and a train of stimulus pulses (200 Hz) delivered through an external bipolar platinum electrode placed across the slice at the midline from a DS2A isolated stimulator (pulses of ∼2–8 V, 0.2 ms; Digitimer, Welwyn Garden City, UK). Connected neurons were identified by a reduction in the 380 nm signal brought about by the postsynaptic rise in calcium concentration resulting from the trains. Cells were then located visually under the microscope and patch clamped.

Whole cell recordings were made from the identified synaptically connected neurons, visualized with 40× or 60× objectives on a Zeiss Axioskop microscope fitted with differential interference phase contrast optics. Patch recordings were made using a multiclamp 700B amplifier and pCLAMP 9.2 software (Molecular Devices), sampling at 50 kHz and filtering at 10 kHz. Patch pipettes were pulled from filamented borosilicate glass (GC150F-7.5, outer diameter 1.5 mm; inner diameter 0.86 mm; Harvard Apparatus, Edenbridge, UK) with a two-stage vertical puller (PC-10 Narishige, Tokyo, Japan). Pipettes were used with final tip resistance ∼3.5 MΩ when filled with a solution containing (mM): 130 CsCl, 5 EGTA, 10 Hepes, 1 $MgCl_2$ and 5 QX314; pH was adjusted to 7.3 with CsOH, osmolarity to 310 mosmol l^{-1} with sucrose. EPSCs in whole cell configuration were elicited by stimulation through the bipolar electrode placed at the midline using the above parameters.

Unless otherwise specified, all recordings were taken at the physiological temperature of 37 ± 1°C, with the bath temperature being feedback controlled by a Peltier device warming aCSF passing through a fast-flow perfusion system, built by the University of Leicester Mechanical and Electronics workshop. A ceramic water-immersion objective coated with Sylgard (Dow-Corning, Midland, MI, USA) was used to minimize local heat loss. EPSCs were elicited at 0.2 Hz to minimize desensitization and short term depression, and in the lower temperature studies, recordings were made in the same cells at the higher temperature to allow the cells to act as their own controls. Current–voltage (I–V) relationships were recorded by varying the holding potentials in increments of 10 mV. A junction potential of 5 mV was subtracted from I–V relationships. Drugs were obtained from Sigma UK, unless specified otherwise. Drugs were applied by bath perfusion in the aCSF: D-AP5, Zn^{2+}, ifenprodil, *N,N,N′,N′*-tetrakis(2-pyridylmethyl)ethylenediamine (TPEN).

Series resistances (R_s) for patch recordings for each age group were similar (MΩ: P9: 6.6 ± 0.5; P11: 5.9 ± 0.4; P14: 5.3 ± 0.3; P18: 5.7 ± 0.8; P21: 5.8 ± 0.7; P35: 7.7 ± 0.5) and compensated by 70%. A voltage error associated with the clamping current passing across the series resistance is unavoidable; this is significant for the large AMPAR-EPSC (mean R_s: 6.1 MΩ; mean voltage error: 19 mV at peak current). Nevertheless this error has little impact on the smaller magnitude and slower time course NMDAR currents. Additionally the AMPAR currents are of similar magnitude across the age range, so any error will be consistent across the different ages and hence have minimal impact on interpretation. No numerical correction has been applied, but the mean series resistances are quoted above for each data set.

Comparison of the charge mediated by AMPAR and NMDAR (and their ratio) at different ages was made for an 'ideal' situation in the absence of voltage-dependent Mg^{2+} block by calculation of the integrals at −65 mV and +45 mV, respectively.

Modelling of the NMDAR current voltage-dependent block

The voltage dependence of whole cell NMDAR-EPSC peak amplitudes were fitted using eqn (1) (Woodhull, 1973; Mayer & Westbrook, 1987; Ascher & Nowak, 1988):

$$I = G(V - V_r)(1 + [Mg^{2+}]_o/K_o \exp(V/V_o)) - 1 \quad (1)$$

where G is conductance, V_r is reversal potential, K_o is apparent Mg^{2+} dissociation constant at 0 mV, V_o is steepness of the voltage dependence, V is command voltage, and $[Mg^{2+}]_o$ is external Mg^{2+} concentration. The curve fits shown in Fig. 7*B* (across a range of external Mg^{2+} concentrations) were estimated with identical parameters between age groups except for K_o. The parameters are stated in Fig. 7*B* legend.

DAR-4M and Fura-2 imaging

Nitric oxide. For loading of DAR-4M, slices were incubated for 30 min in 5 ml of 10 μM DAR-4M AM at room temperature. After loading, slices were postincubated in aCSF for 30 min to allow de-esterification of the AM dye and then transferred to the recording chamber. For measurements of NO production,

DAR-4M was excited at 560 nm and images acquired every 5 s (exposure time: 20 ms). The fluorescence above 575 nm was detected using an IF excitation filter, a DM550 dichroic mirror, and a BA575 emission filter (Nikon, Tokyo, Japan).

Calcium. Slices were loaded with 5 μM Fura 2 AM (Molecular Probes; dissolved in dimethyl sulphoxide (DMSO) containing 5% pluronic acid) for 5–8 min in aCSF. Before recording, slices were kept in aCSF for 30 min to allow de-esterification of the AM dye. Fura 2 fluorescence was detected as described previously (Billups *et al.* 2002) and viewed using a PentaMax intensified CCD camera (Princeton Instruments, Inc., Trenton, NJ, USA). The fluorescence image (emission >505 nm) was displayed using Metafluor imaging software (v. 7, Molecular Devices), and the light source was a Polychrome II Monochromator (TILL Photonics, Martinsried, Germany).

RNA extraction and quantitative real-time PCR analysis

The MNTB was dissected from brain slices (as above) obtained from Lister Hooded rats aged 11, 21 and 34 days and used to extract RNA. Total RNA was isolated from tissue using TRI Reagent (Applied Biosystems, Foster City, CA, USA). cDNA synthesis was performed using random primers and Superscript III (Invitrogen). PCR primers were designed using the Primer Express v. 2.0 Software program (Applied Biosystems). Primers sequences were as follows:

β-Actin forward primer, 5′-GATTACTGCTCTGGCTCCTAGCA-3′, reverse primer, 5′-GTGGACAGTGAGGCCAGGAT-3′; NR2A forward primer, 5′-GTGGTGATCGTGCTGAATAAGG-3′, reverse primer, 5′-ATGCCGCAGGCTCAGAGT-3′; NR2B forward primer, 5′-AGCCAGGAGGCCCATCTT-3′, reverse primer, 5′-GCACAGGTACGGAGTTGTTAAACA-3′ NR2C forward primer, 5′-GCTGCGGAAGGCTTTTTGT-3′, reverse primer, 5′-CTGTCCTTATCGTGCCTTTGTTC-3′; NR2D forward primer, 5′-GGCTCAGCGACCGGAAGT-3′, reverse primer, 5′-TTTCCGTGGACCCATTGG-3′.

Primers were designed to cross exon–exon regions and the gene of interest normalised against a housekeeping gene. qPCR was performed using SYBR Green PCR Master Mix in the ABI PRISM 7700 Sequence Detection System (Applied Biosystems). The thermal-cycler protocol was: stage 1, 50°C for 2 min; stage 2, 95°C for 10 min; and stage 3, 40 cycles at 95°C for 15 s and 60°C for 1 min. Each sample was run in triplicate. Quantification was performed using the comparative C_T method ($\Delta\Delta C_T$) (Livak & Schmittgen, 2001). Data are presented as means ± S.D. ($n = 3$–8 for each group). Statistical significance was assessed as $P < 0.05$ using one-way analysis of variance.

Immunohistochemistry

Lister Hooded rats aged 11, 21 and 34 days old were used. After killing, the brainstem was extracted in ice-cold phosphate-buffered saline (PBS), then transferred to OCT medium and frozen using dry ice and hexane. Transverse cryostat sections (12 μm) were taken from the unfixed tissue and mounted onto poly-lysine coated slides. Sections were fixed in methanol for 5 min at −20°C, then washed 3 × 5 min in PBS with 0.1% Triton X-100. Blocking was performed with 1% BSA and 1% goat serum in PBS with 0.1% Triton X-100 for 1 h at room temperature. Primary antibodies, diluted in blocking buffer, were applied to sections and incubated overnight at 4°C. Mouse anti-Kv3.1b (diluted 1 : 1000, NeuroMab, Davis, CA, USA, cat. no. 73-041, Steinert *et al.* 2008); rabbit anti-NR2A was diluted 1 : 1000 (immunogen sequence a/a 1381–1394; antibody kindly provided by Dr P. Chazot, University of Durham, UK, Cik *et al.* 1993); mouse anti-NR2B was diluted 1 : 500 (immunogen sequence a/a 892–1051; BD Biosciences-Pharmingen, San Diego, CA, USA, Valle-Pinero *et al.* 2007); rabbit anti-NR2C (cat. no. PPS033, R&D Systems, Minneapolis, MN, USA) was diluted 1 : 1000; mouse anti-PSD-95 was diluted 1 : 2000 (immunogen sequence a/a 77–299, cat. no. 73-028, NeuroMab, Davis, CA, USA). Sections were then washed 3 × 10 min in PBS with 0.1% Triton X-100 followed by incubation with secondary antibodies, either Alexa Fluor 488 or Alexa Fluor 546 (goat anti-rabbit 1 : 1000, goat anti-mouse 1 : 500; Molecular Probes) diluted in blocking buffer, for 2 h at room temperature. Negative controls were performed by incubating sections with secondary antibodies while omitting the primary antibody step.

After a final washing step (4 × 10 min), slides were mounted with Vectorshield HardSet Mounting Medium with DAPI (Vector Laboratories, Burlingame, CA, USA). Images were obtained using a Leica fluorescence microscope (DM2500) fitted with a CCD camera (DFC350fx).

For co-staining with mouse anti-NR2B and anti-PSD-95, after incubation with the pooled primary antibodies and subsequent washing, sections were first incubated for 1 h with the secondary antibody specific for isotype IgG2b, goat anti-mouse Alexa Fluor 488 (Molecular Probes) before addition of the non-IgG specific secondary antibody, goat anti-mouse Alexa Fluor 546 (Molecular Probes).

Statistics

Data are presented as means ± S.E.M. and significance verified using Student's two-tailed paired or unpaired *t* test or ANOVA as indicated, with $P < 0.05$ being considered significant.

Results

The aim of these experiments was to examine the development of synaptic NMDA receptors during maturation of the auditory system after the onset of hearing. We have used Lister Hooded rats and CBA/Ca mice to gain greater breadth of experimentation than was possible by using either species alone (see Methods).

NMDAR-EPSCs are larger and faster at physiological temperatures

The evoked EPSC generated by the calyx of Held had a typical dual component response, with a fast AMPAR-mediated component and a slower-time-course voltage-dependent NMDAR-mediated current, as shown in Fig. 1*A*. To aid comparison with published data we first tested the temperature sensitivity of the NMDAR-mediated EPSC by comparing calyceal synaptic responses at 25 and 37°C in the same neurons (Fig. 1*A*; rat P10/11). This clearly shows that the slow EPSC increased in amplitude and had accelerated kinetics when the temperature was raised to 37°C. We confirmed that the slow EPSC is mediated by NMDAR by perfusion of the NMDAR antagonist D-AP5 (50 μM) as shown in Fig. 1*B*. The temperature effect was similar across the whole voltage range as shown by the mean current–voltage (*I–V*) relationship in Fig. 1*C*. We have previously shown that raising temperature increases the amplitude of the fast EPSC by actions on postsynaptic AMPA receptors (Postlethwaite *et al.* 2007) while there is little net effect of temperature on transmitter release (Kushmerick *et al.* 2006). It is clear from Fig. 1*A* that NMDAR current amplitudes were increased at physiological temperatures, by 150% ($n = 3$; HP = +45 mV). This substantial increase in peak current at physiological temperatures suggests that previously NMDAR current magnitudes have been greatly underestimated from *in vitro* experiments conducted at room temperature. All subsequent experiments were conducted at 37–38°C.

The NMDAR-EPSC declines in amplitude and accelerates in time course with development

In order to determine the development time course at physiological temperatures we conducted whole cell patch recordings from rat and mouse MNTB neurons. NMDAR-mediated synaptic currents were present in P10 to P21 rats (Figs 2 and 3) and in P11 to P35 mice (Fig. 3). A decline in NMDAR synaptic current with age is well documented; here we extended the analysis to animals at even more mature ages and found that NMDAR-EPSCs were maintained, but there was a clear acceleration in the EPSC kinetics. *I–V* relationships with 1 mM $[Mg^{2+}]_o$, appeared similar at P11 and P21 and showed the characteristic negative slope conductance associated with voltage-dependent block by Mg^{2+} (but see Fig. 7*B*). The reversal potential was consistent with permeability to non-specific cations, and taking junction potentials into account gave a reversal potential of around +5 mV. The developmental trends of the NMDAR-EPSC

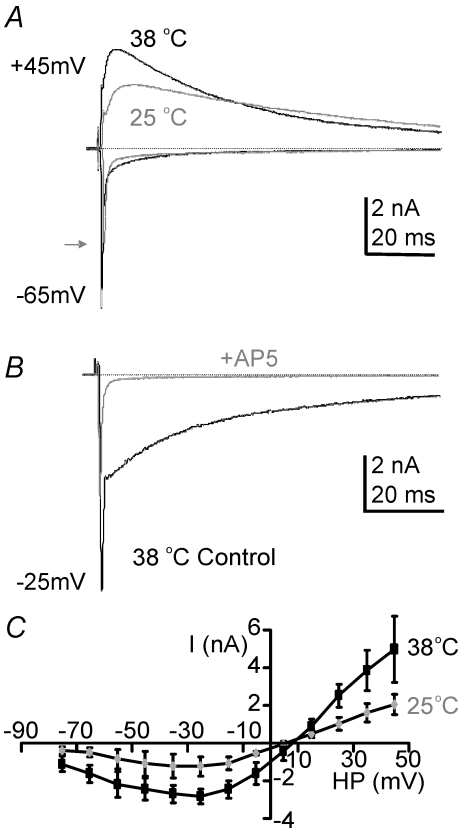

Figure 1. NMDAR-EPSCs double in amplitude on raising experimental temperature from RT to physiological
A, the evoked EPSC at holding potentials of −65 mV or +45 mV for 37°C (black traces) and 25°C (grey traces) recorded from the same MNTB neuron. Zero current is indicated by the dashed line. The grey arrow indicates the peak fast EPSC at 25°C. *B*, superimposed traces from the same cell at a holding potential of −25 mV, before and during perfusion with the specific NMDAR antagonist D-AP5 (50 μM, grey trace). *C*, average current–voltage relationship measured at the peak of the slow EPSC shows the classic voltage dependence block at negative potentials. The potentiation with raised temperature is similar across all voltages, suggesting that the increase is not due to a change in magnesium sensitivity of the NMDAR. Data are means ± S.E.M. from 3 neurons per data point, each measured at both temperatures, from rat calyx of Held/MNTB.

were assessed for both rat and mouse and are presented in Fig. 3.

To aid comparison, the same parameters from rat and mouse MNTB are shown in adjacent plots for each of the six parameters. There are also technical reasons for presenting data from both species: first, obtaining patch recordings from rat MNTB neurons with intact calyceal synapses proved difficult in our hands for rats older than 21 days; second, some of our antibodies for NMDAR subunits were raised in mice and so all the histology was performed on rat tissue. The changes and trends observed between rats and mice over the age range of 14–21 days were very similar, consistent with our conclusions being applicable to both species. The following parameters have been plotted against age from P10–P21 rats and P9–P35 mice: NMDAR-EPSC amplitude, decay time constant and time to peak; AMPAR-EPSC amplitude and decay time constant; and NMDAR/AMPAR charge ratio.

One difference between rat and mouse EPSCs was that the peak amplitude of NMDAR currents was significantly larger in rats at all ages tested (at P11, $P < 0.003$; P14, $P < 0.003$; P18, $P < 0.0001$; P21, $P < 0.0001$; Fig. 3*A* and *G*). This is not a scaling or general 'size' issue, since AMPAR-EPSCs were of similar magnitude (Fig. 3*D* and *J*) in the two species. The AMPAR-EPSC increased in magnitude between P14 and P18; although this was more variable in the rat data, other studies have established an increase in synaptic AMPAR current and density with maturation at the calyx of Held (Joshi *et al.* 2004; Hermida *et al.* 2006). The time course of the various developmental profiles was broadly similar between the two species, with the major changes occurring between days P10/11 and P18. The NMDAR-EPSC amplitude declined and the kinetics accelerated, so that mature NMDAR currents were relatively fast, decaying with a time constant of around 15 ms at 37°C (*versus* 40–50 ms at P10). Although the AMPAR-EPSC provided a much larger peak current, the slow time course of the NMDAR-EPSC generated considerable charge, so that the net charge (in the absence of Mg^{2+} block, see Methods) was always dominated by the NMDAR component even at P35. The charge ratios (NMDA/AMPA) are given in Fig. 3*F* and *L*. The ratio was 2.7 ± 0.8 at P35 for mouse and 7.1 ± 1.5 for P21 rat. These data suggest that NMDAR charge was ∼3 times that of AMPAR in mouse and ∼7 times that of AMPAR in rat at P35/P21. The difference between mouse and rat was due to the larger NMDAR amplitudes in rat (as stated in Fig. 3*A*) and similar AMPAR amplitudes. This will have a major impact on signalling at this synapse (see below). For the mouse we were able to extend the recordings out to 35 days postnatal and this further 2 weeks of development showed no significant difference from the P18 animals. This provides two important conclusions. First, NMDAR-mediated EPSCs decline but are maintained on maturation beyond hearing onset. Second, the vast majority of development at this level of the auditory system has occurred by 18 days postnatal. Thus we can conclude that the mature calyx of Held synapse is mediated by both NMDARs and AMPARs; currents through AMPARs are around 10 nA

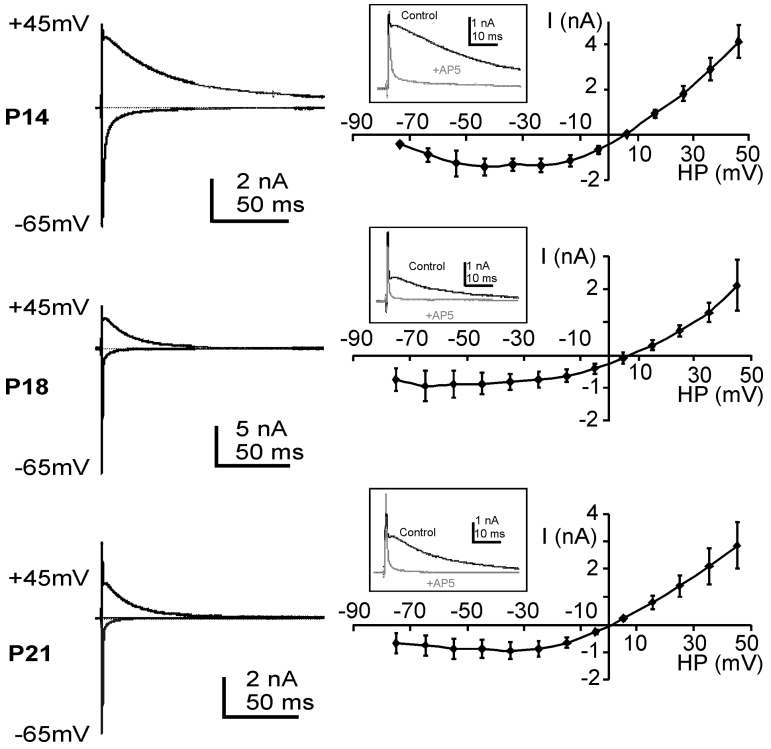

Figure 2. The NMDAR-EPSC shows declining amplitude and accelerating decay during maturation
Example EPSCs for +45 mV and −65 mV holding potentials are shown superimposed (left) for examples recorded from rat MNTB neurons at P14, P18 and P21. The mean *I–V* relationships (non-isochronal) for the NMDAR-EPSC are shown (right) for the same ages. Insets show example traces at positive holding potentials demonstrating block of the outward slow EPSC current by the NMDAR antagonist AP-5. Data are means ± S.E.M. from 3 neurons per data point from rat calyx of Held/MNTB recordings.

in amplitude, but decay with a time constant of around 0.3 ms, while currents through NMDARs are in the region of 300–500 pA and have a time constant of 15 ms (NMDAR: P21 mouse: 353 ± 51 pA/15 ± 2 ms; and P35 mouse: 290 ± 105 pA/16 ± 4 ms). Hence although NMDAR-EPSCs are much smaller in amplitude, they would contribute a greater overall charge, were it not for voltage-dependent Mg^{2+} block at resting potentials (see Discussion).

The contrast between the NMDAR-EPSCs generated in P12 *versus* P35 mice are shown in superimposed data from the two ages at holding potentials of +45 and −65 mV (Fig. 4*A*). Confirmation of the slow component being mediated by NMDAR is provided by block with D-AP5 (50 μM; Fig. 4*B*). Although there is a considerable decline in the size of the NMDAR-mediated response from P9 to P35, the high frequencies of auditory stimulation mean that summation of NMDAR-EPSCs is relevant at all ages (Fig. 4*C*; the grey shading indicates the cumulative NMDAR currents during repetitive synaptic stimulation).

Decreased amplitude and accelerating time course suggest increased NR2A over NR2B subunits

The acceleration of the NMDAR-EPSC kinetics with development suggests that there are important changes occurring in the modulation and/or subunit composition of sub-synaptic NMDA receptors during maturation. We used real time PCR and immunohistochemistry to test for changes in mRNA and protein expression.

The immunohistochemistry was conducted in the rat using tissue from animals of the indicated ages. It has previously been demonstrated that antibodies to the potassium channel Kv3.1 provide a clear definition of the MNTB nucleus and its principal neurons (Li *et al.* 2001; Song *et al.* 2005). Co-localisation of Kv3.1b antibodies with NR2A showed that they were present in MNTB principal neurons (Fig. 5). Double labelling with antibodies to NR2A, NR2B or NR2C (green) with PSD-95 (red) showed clear localisation to cell body cytoplasm and membrane in the principal neurons. Non-principal neurons and glial cells had little or no somatic PSD-95 or Kv3.1b labelling. NR2A, NR2B and NR2C were located on MNTB principal neuron plasma membranes, but comparison between the subunits was not possible (because the antibodies were raised in the same host species). Similar observations were made in three animals. Staining was observed in P11, P21 and P34 animals; although there was qualitatively more intense staining in younger animals (see Supplemental Fig. 1), some staining was observed for each of the sub-units at all ages. Although cytoplasmic staining was prevalent, more intense staining was observed in the plasma membrane, as shown by the line plots (Fig. 5*C*).

qPCR was conducted in rat MNTB tissue dissected from animals aged P10, P21 and P35. The observations are consistent with the electrophysiology and immunohistochemistry, showing a large relative increase in mRNA for NR2A and little change in NR2D message with age (Fig. 6). NR2B message peaked between P10 and P21, while NR2C increased later, between P21 and P35. It is not possible to compare relative expression levels between subunits, but these changes in message are consistent with a shift to NR2A- and NR2C-containing subunits with maturation.

These observations show that NMDARs contribute to synaptic transmission at the mature calyx of Held. Our results give four new insights into NMDAR function at this level of the auditory pathway. (1) Synaptic NMDAR currents are larger at physiological temperatures compared to room temperature (RT). (2) The NMDAR-EPSC declines in amplitude following hearing onset by around 85% (P11 *vs.* P21) in mouse and 53% in rat (P11 *vs.* P21), but is not eradicated. (3) Accompanying the declining amplitude, the kinetics of the NMDAR-EPSC decay accelerate (time to peak is shorter and decay τ is faster). (4) The dominance of the AMPAR-EPSC in triggering postsynaptic action potentials is clear, but the charge transfer (rather than peak amplitude) shows a 3- or 7-fold larger charge (mouse *vs.* rat) passing through synaptic NMDARs; nevertheless this makes little or no contribution to excitability (Futai *et al.* 2001), suggesting that NMDARs at mature synapses couple to non-electrical forms of signalling such as nitrergic signalling (Steinert *et al.* 2008).

Synaptic channels include NR2A and NR2C subunits

Closer examination of the pharmacology of NMDAR-mediated EPSCs during development of the calyx of Held revealed some new elements to the maturation. In common with many synapses across the brain, higher sensitivity to ifenprodil (NR2B antagonist) was noted in young animals (Joshi & Wang, 2002). After opening of the auditory canal we saw little or no sensitivity to ifenprodil by P18 (Fig. 7*A*), suggesting that NR2B subunits no longer contributed to sub-synaptic receptors. The faster EPSC kinetics observed on maturation were also consistent with NR2A subunit expression. However, sensitivity to extracellular zinc (200 and 500 nM) was not detected and the Zn^{2+} chelating agent TPEN (10 μM) also had no effect, which suggests the NR1-1b spliced variant is expressed in the MNTB. In addition to the decline in amplitude from P11 to P18, sensitivity to $[Mg^{2+}]_o$ declined (Fig. 7*B*). At P11 synaptic NMDARs were more sensitive to voltage-dependent block than at P18, as shown by the reduced block in 0.1 mM $[Mg^{2+}]_o$. The data were fitted to eqn (1) (see Methods) for all

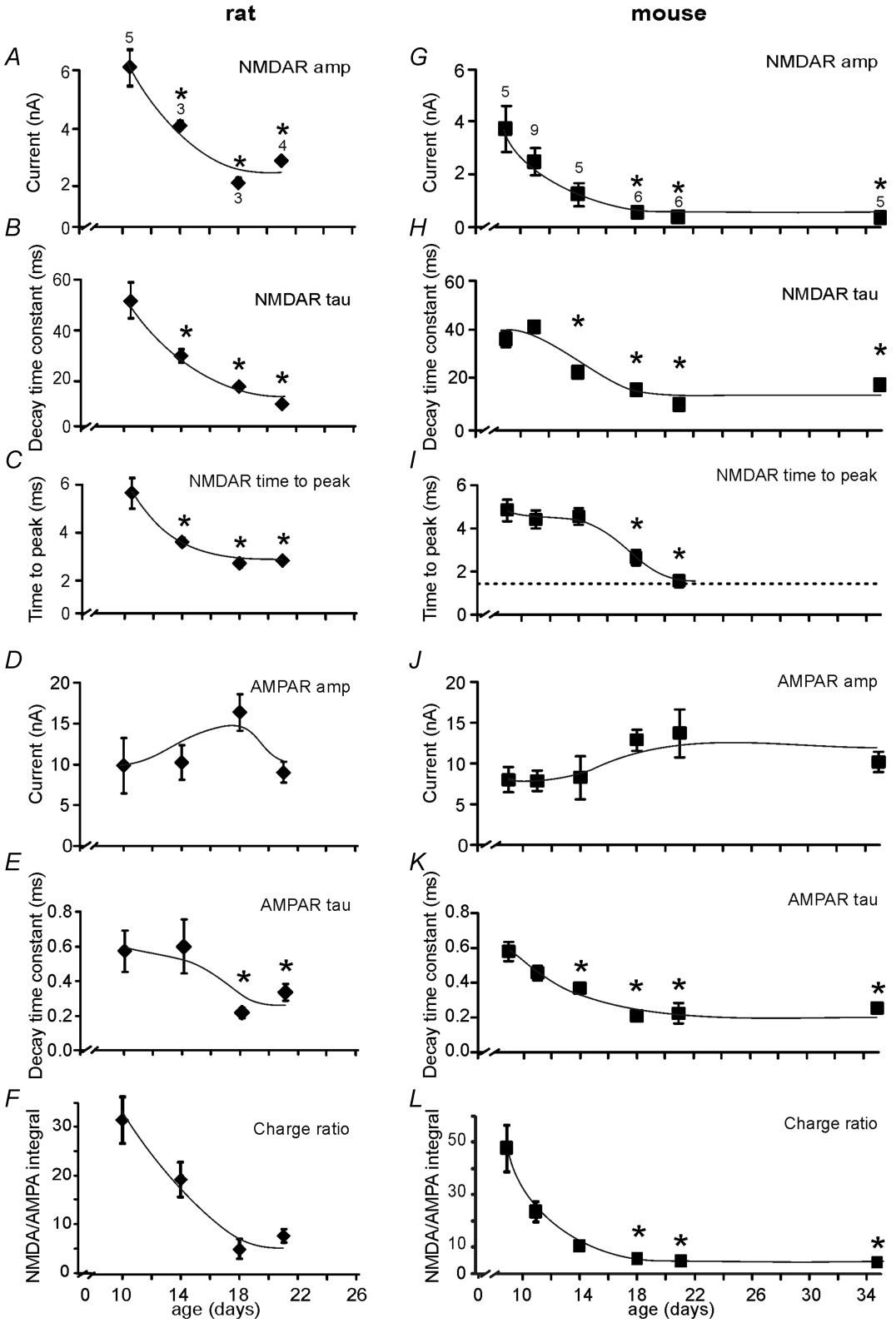

Figure 3. Development of fast-AMPAR and slow-NMDAR-EPSCs generated in response to stimulation of the calyx of Held of rat (left, *A–F*) and mouse (right, *G–L*)

A and *G*, NMDAR-EPSC amplitudes decay from P10/11 (rat) and P9 (mouse) until P18. NMDAR peak currents were measured at +45 mV. *B* and *H*, slow-EPSC decay time constants accelerate until P18–P21. *C* and *I*, the time to peak of the slow EPSC also accelerates until P21 (note that P35 values in mice were so fast that they

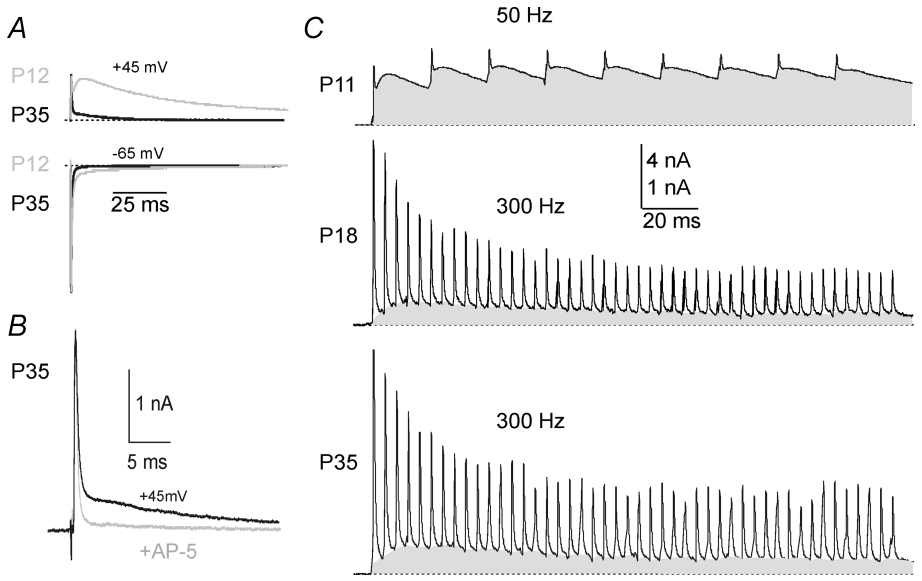

Figure 4. NMDAR-EPSCs are maintained at mature calices from P35 mice
A, superimposed EPSCs from animals aged P12 (grey) or P35 (black) illustrating the large decrease in NMDAR-EPSC amplitude and faster kinetics (+45 mV, top traces, −65 mV, bottom traces). *B*, the slow EPSC at P35 is blocked by perfusion of the NMDAR antagonist D-AP5 (grey trace, HP = +45 mV). *C*, summation of NMDAR-EPSCs is an important element of NMDAR activation under physiological conditions; zero current indicated by dashed line, grey areas indicate accumulation of the slow-EPSC/NMDAR currents for P11 (50 Hz), P18 (300 Hz) and P35 (300 Hz) (HP = +45 mV). Data are from mouse calyx of Held/MNTB.

$[Mg^{2+}]_o$ and at two ages (P11 and P18) as illustrated by the continuous lines in both *I–V* curves in Fig. 7*B*. The required fitting parameters showed a twofold increase in the apparent dissociation constant of Mg^{2+} at 0 mV (K_o) (P11: $K_o = 7.5$ mM; and P18: $K_o = 14$ mM) confirming a reduced Mg^{2+} sensitivity at older ages. All other parameters (conductance, *G*; steepness of voltage dependence, V_o; reversal potential, V_r) were kept constant and their values were consistent with previous reports (Mayer & Westbrook, 1987; Ascher & Nowak, 1988). Such a decline in magnesium sensitivity is consistent with increased expression of NR2C/D subunits. The fast kinetics and low level of message made the presence of NR2D unlikely, but the incorporation of NR2C subunits is supported by the PCR and immunohistochemistry (Figs 5 and 6).

These observations reinforce the idea that there are two changes in subunit expression during maturation of NMDARs at the calyx of Held: there is a decline in NR2B containing channels after opening of the auditory canal, and then there is an additional incorporation of NR2C subunits by P18. Immunohistochemical studies confirmed that NR2A, NR2B and NR2C subunits were present in the MNTB and were associated with postsynaptic densities in that there was co-localisation with PSD-95.

Analysis of the NMDAR-EPSC decay time constants showed a fast and slow component. The time constant τ_{fast} accelerated from 25 ms to around 10 ms from P11 to P35 and accounted for around two-thirds of the peak amplitude at all ages (Fig. 8*A*). The time constant τ_{slow} also changed from around 100 ms to 50 ms (Fig. 8*B*). The time course of the age-related decline in amplitude and accelerated kinetics were remarkably similar for both fast and slow components and so the amplitude ratio of the fast and slow time course currents remained stable over this developmental period (Fig. 8). In addition there was no evidence that the two time constants were differentially affected by ifenprodil, Zn^{2+} or Mg^{2+} (data not shown) suggesting that the dual decay kinetics reflect openings of a single channel population, rather than the differing kinetics of two independent heteromeric channel populations.

showed no distinct peak). *D* and *J*, fast AMPAR-EPSC amplitudes (measured at −65 mV) increase from P14 to P18; however, the data from rat appear to show a decline again at P21. *E* and *K*, fast EPSC decay time constants accelerate. *F* and *L*, NMDAR-EPSC to AMPAR-EPSC charge ratios were calculated at positive (+45 mV) and negative voltages (−65 mV), respectively (see Methods). Significance was tested using ANOVA followed by a *post hoc* test, *Significance relative to youngest age. Data are means ± S.E.M. from 3–9 cells per data point (n = number of cells and is indicated above the data points in *A* and *G*). *Statistical significance was accepted if $P < 0.05$; data are from rat and mouse calyx of Held/MNTB neurons.

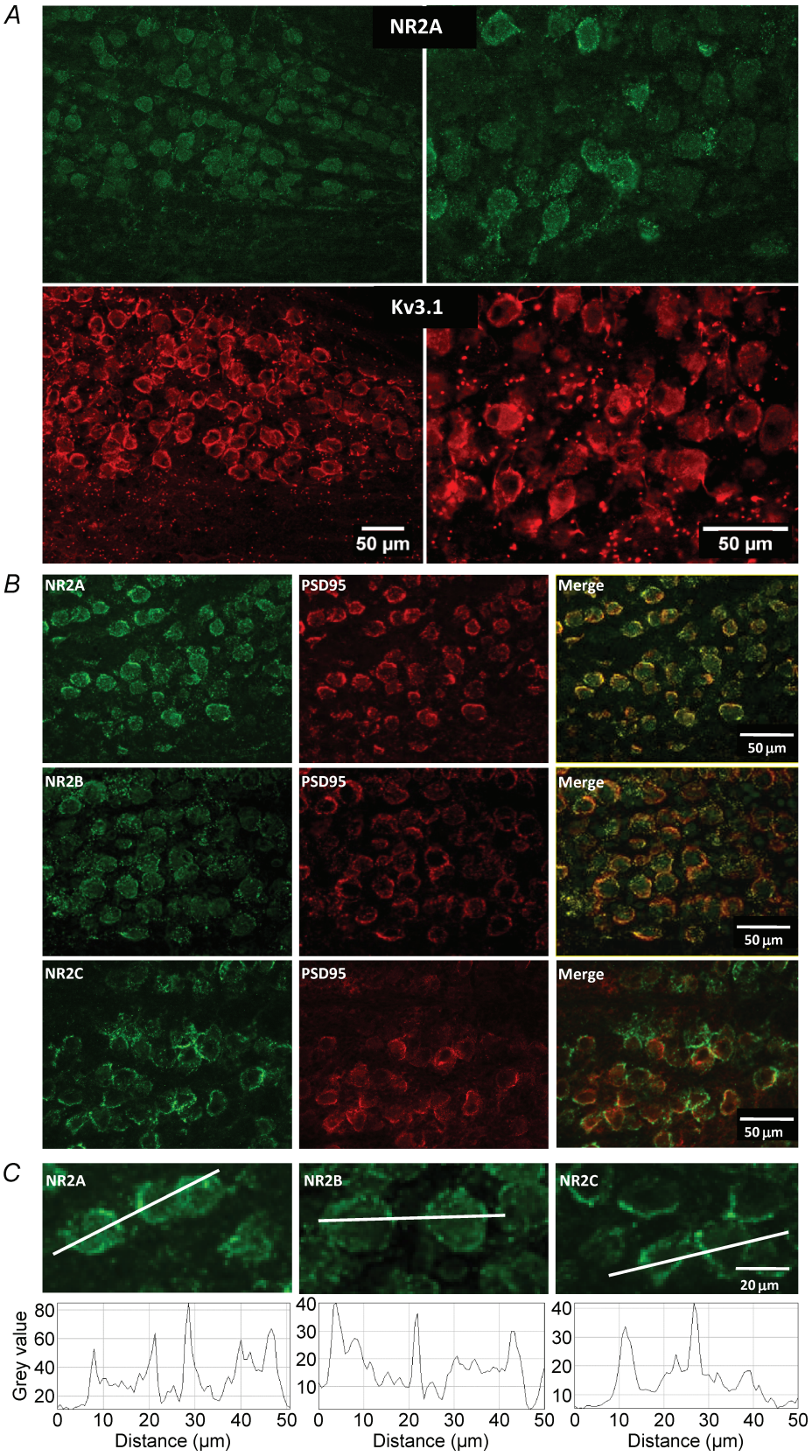

Figure 5. Immunohistochemical labelling indicates that NR2A, NR2B and NR2C are present in the MNTB
A, co-localisation of NR2A (green, top) and Kv3.1b (red, bottom); both left (20× magnification) and right

Although the impact of the NMDAR on the electrical signalling is small, other forms of signalling may be more important at the mature synapse (>P36), so we performed calcium and nitric oxide imaging experiments. Application of two synaptic stimulation protocols (SSPs) elicits robust nitric oxide generation at younger (Steinert *et al.* 2008) but also at mature MNTB neurons (Fig. 9). The images in Fig. 9*A* show three MNTB neurons (Fura 2 fluorescence at 380 nm, left) of which two receive a synaptic input which generates postsynaptic Ca^{2+} increases (red traces) on synaptic stimulation. When imaging the DAR-4M fluorescence before (Ctrl, middle) and after synaptic stimulation (SSP, right), a substantial increase in fluorescence was observed. This increase is plotted over time in Fig. 9*B* for a control recording with two repeated SSPs and for a recording in which 50 μM AP-5 and 10 μM MK801 were applied after the first SSP but prior to the second. Both of the SSP stimuli evoked DAR-4M fluorescence (ΔF_1 and ΔF_2 measured 1000 s after stimulation), but after incubation with NMDAR antagonists the second SSP response (ΔF_2) was reduced indicating a contribution from NMDARs. This changed response was seen as a smaller ratio of $\Delta F_2/\Delta F_1$ (Fig. 9*C*). NMDARs at the mature synapse showed faster decay kinetics than at the immature synapses, so it was expected that low frequency trains of stimulation (~100 Hz) would lead to little cumulative activation, whereas higher frequencies (~400 Hz or above) should cause a substantial cumulative activation of NMDARs. To investigate this frequency dependency we performed the above experiments using SSP trains with different frequencies (100 Hz *vs.* 400 Hz). As shown in the summary graph in Fig. 9*C*, the effects of NMDAR inhibition (AP-5/MK801) were greater with higher frequency stimulation, as illustrated by the stronger reduction in $\Delta F_2/\Delta F_1$ ratios.

Involvement of Ca^{2+} in NO generation was confirmed by measurement of Fura 2 ratios (plateau values of a 200 Hz train) on synaptic stimulation at P12 and P31 (Supplemental Fig. 2). Application of AP-5/MK801 reduced Fura 2 ratios in both P12 and P31 animals to a similar extent, suggesting that total Ca^{2+} influx through NMDARs was similar despite the 10 times smaller NMDAR whole cell currents at mature synapses. Inhibition of AMPARs and NMDARs together (Supplemental Fig. 2) abolished any Ca^{2+} influx. Furthermore, blocking AMPARs alone (10 μM NBQX) eliminated any Ca^{2+} response as expected due to the lack of depolarisation (data not shown).

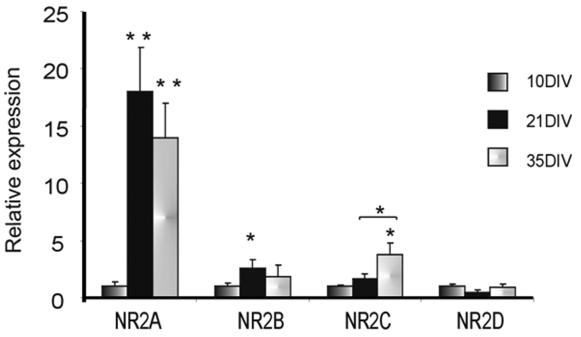

Figure 6. Changes in relative expression of NR2 mRNA using qPCR in MNTB during development
Total RNA was isolated from animals at P10, P21 and P35 and gene expression was estimated by qPCR. NR2A shows the largest relative increase by P21, with NR2C also showing significant increases later in development. Statistically different: $^*P < 0.05$, $^{**}P < 0.01$. Data are from rat MNTB.

Discussion

These results confirm that synaptic NMDAR currents decline during maturation after opening of the auditory canal, but they do not disappear. The decline in amplitude is accompanied by a considerable acceleration of kinetics compared to those observed in neurones from younger animals, so that the mature synaptic NMDAR has a decay τ of 10–15 ms. The immunohistochemistry shows NR2A, NR2B and NR2C subunits are present, but the pharmacology does not support incorporation of the NR2B subunits. The mature NMDAR-EPSC is insensitive to $[Zn^{2+}]_o$ and ifenprodil and exhibits less sensitivity to block by $[Mg^{2+}]_o$, consistent with dominant contributions from NR2A and NR2C subunits and minimal contribution of NR2B subunits to synaptic NMDAR channels.

NMDAR-mediated EPSCs are maintained on maturation

Previous studies of the temperature dependence of AMPAR-mediated synaptic transmission indicate that the increase in EPSC amplitude on rising from RT to physiological temperatures is mediated by a raised probability of the channel entering the highest conductance states (Postlethwaite *et al.* 2007); that is a postsynaptic change, rather than a presynaptic increase in transmitter release (Kushmerick *et al.* 2006). A recent study of the temperature dependence of NMDAR also shows increased single channel conductance with temperature while

(40× magnification) MNTBs are shown from the same section of a P21 rat. *B*, co-labelling with antibodies for NR2A (top, green), NR2B (middle, green) or NR2C (bottom, green) with PSD-95 immunostaining (red). On the right merged images. *C*, higher magnification images of NR2A, NR2B and NR2C immunostaining with line scans of intensity shown below each image. Data are from rat MNTB.

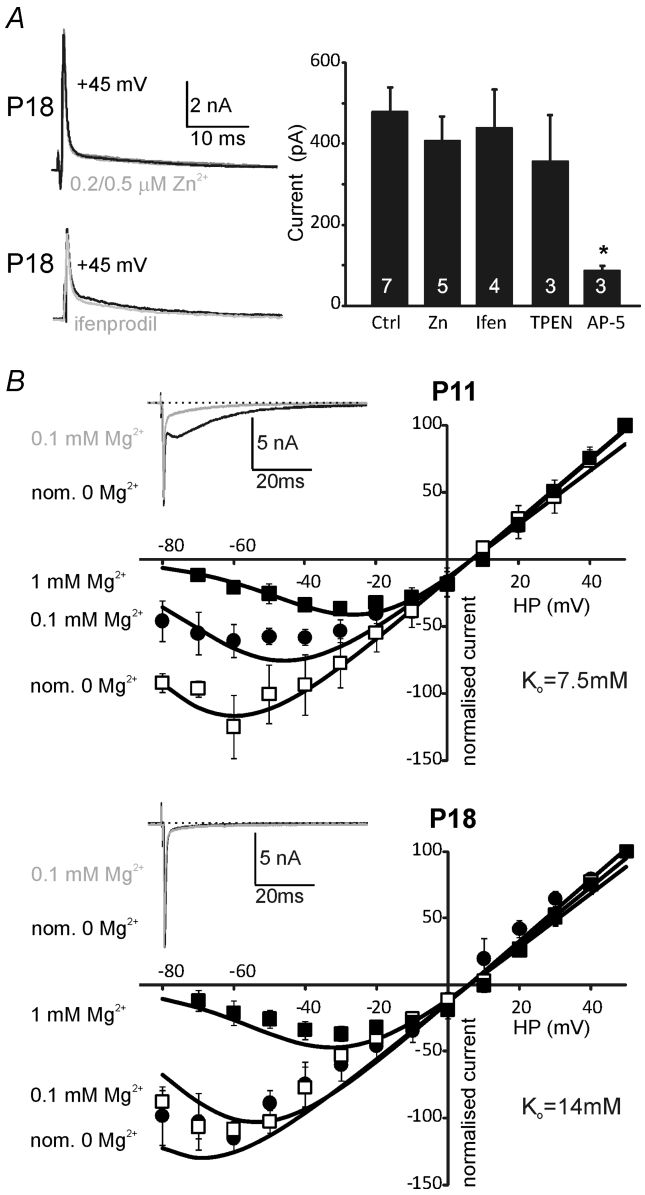

Figure 7. P18 NMDA-EPSCs are insensitive to $[Zn^{2+}]_o$ and ifenprodil and show reduced sensitivity to block by $[Mg^{2+}]_o$
A, two example traces of NMDAR-EPSC recorded at +45 mV under control conditions and during perfusion of 0.5 μM Zn^{2+} (upper, grey trace) or ifenprodil (lower, grey trace). Bar graph summarises this pharmacology under the indicated conditions in P18 mice. The NMDAR-EPSC is insensitive to 0.2–0.5 μM Zn^{2+}, ifenprodil (10 μM, Ifen) and the Zn^{2+} chelator TPEN (10 μM) but is blocked by D-AP-5 (50 μM). n = number of cells, indicated on the bars. *B*, voltage-dependent block by extracellular Mg^{2+} at P11 (upper *I–V* curve) and P18 (lower *I–V* curve). Both *I–V* curves show NMDAR-EPSCs with 1 mM $[Mg^{2+}]_o$ (filled squares, averaged data from mouse and rat, $n = 5$), and for 0.1 mM (filled circles, mouse, $n = 3$) or nominally Mg^{2+} free (assuming 35 μM contaminating Mg^{2+}, open squares, mouse, $n = 4$). Insets show appropriate example traces at a holding potential of −65 mV for the indicated $[Mg^{2+}]_o$. Continuous lines show data fits by eqn (1) with identical parameters at both ages, except for K_o. $V_r = 6$ mV, $G = 5$ μS (normalised), $V_o = 15$ mV; P11: $K_o = 7.5$ mM, P18: $K_o = 14$ mM. Data are means ± S.E.M. Significance was tested using ANOVA, $^*P < 0.05$.

desensitisation was particularly temperature dependent (Cais *et al.* 2008).

The argument for the developmental decline in NMDAR currents in the auditory pathway was based on extrapolation of the decline seen soon after hearing onset and based on the idea that once synaptic connections have been established, there is little need for plasticity and hence little need for NMDA receptors. There is no doubt that NMDAR-EPSCs dramatically decline during synapse maturation, but our results clearly show that NMDAR transmission is not eradicated and is maintained in a mature and functional state.

It is often assumed that a large NMDAR conductance implies large physiological impact and hence a decline indicates decreasing significance; however this is too simplistic, since this receptor is providing signalling in multiple ways, including depolarisation, voltage-dependent block or unblock, conductance and calcium permeability. The signalling will also be influenced by rates of synaptic activity, summation and coupling to downstream pathways. It is clear that the decline in NMDAR currents during early development contributes to increased fidelity of transmission (Taschenberger & von Gersdorff, 2000; Futai *et al.* 2001; Joshi & Wang, 2002); we now extend these observations to later developmental stages and show that the decline in magnitude is associated with changes in subunit composition favouring weaker Mg^{2+} block in mature animals, while the reduced conductance does not necessarily imply a reduced relevance, since it could also be associated with tighter coupling to the second messenger action of Ca^{2+} signalling.

Synaptic NMDAR EPSCs have a fast time course

The time course of these auditory NMDAR-EPSCs is faster than NMDAR-EPSCs reported from elsewhere in the brain and reflects the intrinsic kinetics of the NMDAR rather than glutamate release or uptake (Lester *et al.* 1990; Popescu & Auerbach, 2003). Previous studies of AMPAR in the MNTB also demonstrated fast kinetics associated with expression of GluRDo subunits (Barnes-Davies & Forsythe, 1995; Geiger *et al.* 1995; Joshi *et al.* 2004). Our observations suggest that the mature NMDAR in the auditory pathway may also be specialised for high frequency firing in that the NMDAR-EPSC has an unusually rapid time course by P18. This is consistent with the high evoked and spontaneous firing rates generated in the auditory pathway (Kopp-Scheinpflug *et al.* 2008) and would lead to sustained NMDAR activation during high frequency firing, as we observed during repetitive stimulation (see Fig. 4). Nevertheless this NMDAR current is not triggering additional APs and so is essentially electrically 'silent'. There are no reports of long-term

synaptic plasticity in the MNTB, but NMDARs are closely coupled to NO signalling and modulating postsynaptic excitability (Steinert *et al.* 2008) at the mature synapse.

Changing receptor subunits underlie NMDAR-mediated EPSCs

Identification of native channel subunits is difficult and caution is warranted in interpreting our results as we are dealing with an indeterminate heterogeneity. Our electrophysiological approach, using synaptic stimulation has the overriding advantage of studying NMDAR excitation at the synapse and the use of co-labelling with PSD-95 and NMDAR antibodies has provided complementary evidence of receptor protein at post-synaptic densities. The qPCR data cannot assist in detecting particular subunits that may be of greater synaptic relevance, but comparison of mRNA levels during maturation provides additional evidence about which subunit transcripts are changing and hence indicate those subunits that may be of most relevance. These data confirm a large increase in the relative copy number of NR2A mRNA on maturation of MNTB neurons, along with a smaller increase in levels of NR2C. NR2D subunits are associated with a very long time course and slow kinetics (Brothwell *et al.* 2008), but levels of NR2D mRNA are low and show little or no change with maturation, consistent with *in situ* hybridisation which reported little or no NR2D in the rat MNTB (Sato *et al.* 1999).

The acceleration of the slow NMDAR-EPSC kinetics with maturation is consistent with increased NR2A and reduced incorporation of NR2B subunits as observed in NR2B knockouts (Tovar *et al.* 2000). Absence of NR2B subunits is consistent with lack of block by ifenprodil at P18, and contrasts with data from P14 animals which showed a 20% block by ifenprodil (Joshi & Wang, 2002). The reduction in voltage-dependent block by extracellular magnesium is indicative of NR2C or NR2D containing channels (Momiyama *et al.* 1996). We also see a clear association of NR2C immunostaining with postsynaptic densities. However, the time course of the NMDAR-EPSC currents at the mature calyx of Held are much faster than reports of recombinant NR1/NR2C channels, which have fast activation, but relatively slow kinetics (deactivation around 320 ms, Dravid *et al.* 2008). However, NR2C kinetics are accelerated by phosphorylation (Chen *et al.* 2006), which might explain the discrepancy, particularly in combination with NR1 subunits incorporating exon 5, and may be further accelerated when part of a heterotrimer incorporating NR2A subunits.

There are three NR1 spliced variants expressed in the MNTB (NR1a > 1b > 1–4 and 11) but NR1–3 was not detected (Nakagawa *et al.* 2000). The NR1-1b spliced-variant containing exon 5 is associated with a somatic location (Pal *et al.* 2003) and fast deactivation

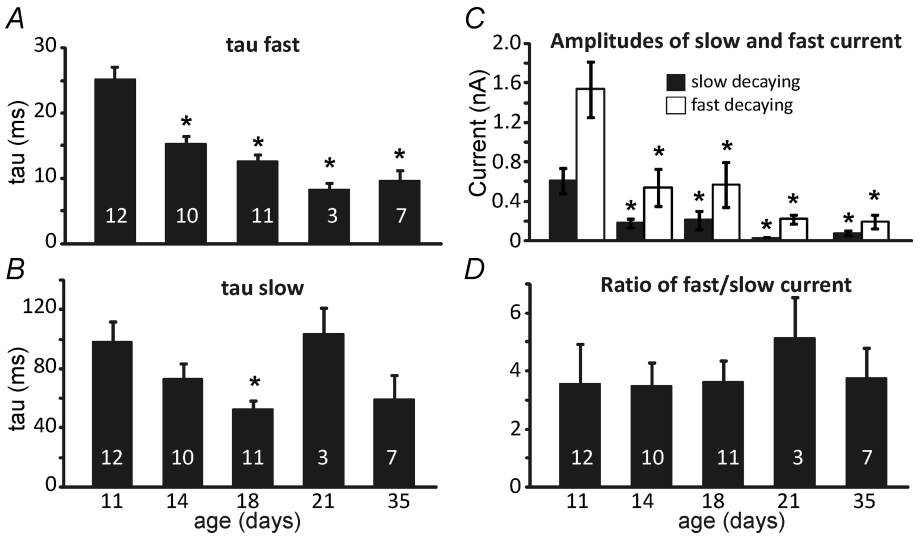

Figure 8. Changes in NMDAR-EPSC kinetics are similar for both the dominant fast and the minor slow time constants

The mean fits to the slow EPSC decay time constants are plotted across P11 to P35 mice. *A*, τ_{fast}; the fast τ shows significant acceleration with maturation from P14 onwards (ANOVA, $P < 0.05$). There are no kinetic changes of the fast decaying current from P14. *B*, τ_{slow}; the slow τ does not show significant changes with age. *C*, the absolute amplitudes of the slow and fast components are plotted against age. Both components decline in amplitude but the ratio of fast : slow is unchanged as shown in *D*. Data are means ± S.E.M., n = number of cells indicated in bars, *Statistical significance, $P < 0.05$. Significance was tested using ANOVA; data are from mouse. All recordings were made with a holding potential of +45 mV for NMDAR currents.

kinetics (Rumbaugh *et al.* 2000). This is also consistent with lack of Zn^{2+} modulation (Traynelis *et al.* 1998) of the EPSC, although this will also be influenced by inclusion of NR2C, which has low Zn^{2+} sensitivity (Rumbaugh *et al.* 2000). An inconsistency here is the extent to which channels incorporating NR2A subunits could be resistant to Zn^{2+} block; but recent work has demonstrated extracellular proteolytic modification removes Zn^{2+} block of NR2 subunits (Yuan *et al.* 2009; Samson *et al.* 2008) and recordings of calyceal responses from tissue plasminogen activator (tPA) knockout mice (kindly provided by Robert Pawlak) also showed no Zn^{2+} sensitivity (data not shown), suggesting this proteolytic mechanism does not account for the lack of Zn^{2+} block here.

It seems unlikely that there are separate NR1–NR2A and NR1–NR2C channel populations, since heterodimeric recombinant channels have distinct properties and both of the NMDAR-EPSC decay components showed similar pharmacology and age-dependent changes (as shown in Fig. 8). The presence of NR2C in the MNTB is consistent with evidence from cerebellar granule cell (Cathala *et al.* 2003) and, intriguingly, granule cells in tissue culture show a similar activity-dependent switch from NR2B to NR2C expression (Iijima *et al.* 2008). Data from recombinant heterotrimers (NR1-1a–NR2A–NR2C; Hatton & Paoletti, 2005) are consistent with the present data, but the lack of Zn^{2+} block in the MNTB suggests that Zn^{2+} is not a universal NMDAR modulator and supports the incorporation of NR1-1b subunits. Proof of the native channel composition at this identified synapse is absent, but the results support the postulate that the NMDAR channel at the calyx of Held–MNTB synapse is a heterotrimer receptor containing NR1-1b–NR2A–NR2C subunits.

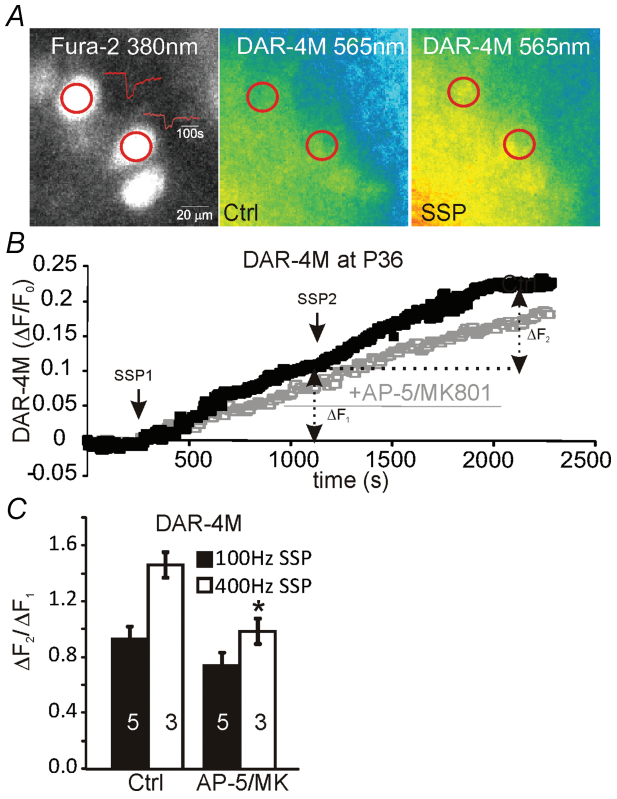

Figure 9. NO generation on synaptic stimulation in MNTB neurons from P36–P40 mice
A, 3 MNTB neurons (fluorescence at 380 nm, left) out of which 2 receive a synaptic input which generates postsynaptic Ca^{2+} increases (red traces) on synaptic stimulation. The two DAR-4M images show fluorescence before (Ctrl, middle) and after synaptic stimulation (SSP, right). *B*, DAR-4 M fluorescence is plotted over time for a control recording with two repeated SSPs (synaptic stimulation protocol [100 Hz trains for 500 ms repeated at 1 Hz for 60 s]) and a recording in which 50 μM AP-5 and 10 μM MK801 were applied prior to the second SSP leading to a reduced response to the second SSP. Repetition of a SSP shows the bi-phasic increase in DAR-4M fluorescence (ΔF_1 and ΔF_2 measured 1000 s after stimulation), and after incubation with NMDAR antagonists (50 μM AP-5, 10 μM MK801) the second phase (ΔF_2) is reduced. *C*, ratios of $\Delta F_2/\Delta F_1$ for different stimulation frequencies (100 Hz and 400 Hz); following NMDAR antagonist incubation this ratio shows a stronger reduction. Data are means ± S.E.M., n = number of cells indicated in bars. Significance was tested using Student's t test, $^*P < 0.05$ relative to Ctrl.

Electrical *versus* second-messenger signalling via synaptic NMDA receptors. Because of the technical difficulties, there are relatively few *in vitro* MNTB recordings from animals older than P18. Previous recordings from P27 mice clearly show a small NMDAR-mediated EPSC (Futai *et al.* 2001), which was likely to have been underestimated because the recordings were performed in 20 μM CNQX, a concentration known to inhibit NMDAR responses by interaction with the glycine binding site (Birch *et al.* 1988; Lester *et al.* 1989). Our work clearly shows that development does not eliminate functional NMDARs in mature rats and mice. There are three important functional points to emphasise. First, although the mature NMDAR-EPSC amplitude is small, the charge transfer (in the absence of Mg^{2+} block) is larger than the AMPAR component, because the NMDAR kinetics of MNTB neurons (while fast for NMDARs) are long-lived relative to the GluRDo-containing AMPAR expressed here. Second, Ca^{2+} imaging experiments reveal that the Ca^{2+} influx at P12 and P31 is similar and that NMDAR contribution to Ca^{2+} influx does not differ between young and mature animals (Supplemental Fig. 2) despite the strongly reduced NMDAR current, suggesting that the relative Ca^{2+} influx in the mature animal must be greater. Third, the close coupling of the NMDAR to nNOS in the postsynaptic density, through their mutual PDZ binding domains (Kornau *et al.* 1995), raises the efficacy by which NMDAR-mediated calcium influx can trigger NO generation, as confirmed by imaging NO generation following synaptic stimulation in animals between P36

and P40. There is a greater NMDAR-sensitive contribution to NO generation at higher frequency trains of stimulation (400 Hz), which reflects accumulation of fast inactivating NMDARs within the train.

These changes are consistent with a developmental shift of NMDAR from electrical conductance signalling in young animals to calcium second messenger signalling on maturation. An important element of this signalling is the enhanced relief of Mg^{2+} block on depolarisation of the synaptic NR2C containing receptors, so that each AP can provide greater Ca^{2+} influx through these NMDARs (Spruston *et al.* 1995; Bollmann *et al.* 1998). Hence the mature synaptic NMDAR could generate more tightly coupled calcium influx compared to the immature synapse, where NMDARs have higher affinity for Mg^{2+}, as indicated by their 2-fold lower K_o. Incorporation of NR2A subunits may also favour greater relative Ca^{2+} influx (Burnashev *et al.* 1995). Despite the reduced total NMDAR current amplitude these adaptations would mediate precisely targeted Ca^{2+} signalling at the postsynaptic density of mature synapses and more efficient coupling to nNOS (Steinert *et al.* 2008), consistent with the hypothesis that synaptic NMDAR function shifts from depolarisation- to Ca^{2+}-dominated signalling.

References

Aamodt SM & Constantine-Paton M (1999). The role of neural activity in synaptic development and its implications for adult brain function. *Adv Neurol* **79**, 133–144.

Ascher P & Nowak L (1988). The role of divalent cations in the *N*-methyl-D-aspartate responses of mouse central neurones in culture. *J Physiol* **399**, 247–266.

Barnes-Davies M & Forsythe ID (1995). Pre- and postsynaptic glutamate receptors at a giant excitatory synapse in rat auditory brainstem slices. *J Physiol* **488**, 387–406.

Billups B, Wong AC & Forsythe ID (2002). Detecting synaptic connections in the medial nucleus of the trapezoid body using calcium imaging. *Pflugers Arch* **444**, 663–669.

Birch PJ, Grossman CJ & Hayes AG (1988). 6,7-Dinitro-quinoxaline-2,3-dion and 6-nitro,7-cyano-quinoxaline-2,3-dion antagonise responses to NMDA in the rat spinal cord via an action at the strychnine-insensitive glycine receptor. *Eur J Pharmacol* **156**, 177–180.

Bliss TV, Collingridge GL & Morris RG (2003). Long-term potentiation and structure of the issue. *Philos Trans R Soc Lond B Biol Sci* **358**, 607–611.

Bollmann JH, Helmchen F, Borst JG & Sakmann B (1998). Postsynaptic Ca^{2+} influx mediated by three different pathways during synaptic transmission at a calyx-type synapse. *J Neurosci* **18**, 10409–10419.

Brew HM & Forsythe ID (1995). Two voltage-dependent K^+ conductances with complementary functions in postsynaptic integration at a central auditory synapse. *J Neurosci* **15**, 8011–8022.

Brothwell SL, Barber JL, Monaghan DT, Jane DE, Gibb AJ & Jones S (2008). NR2B- and NR2D-containing synaptic NMDA receptors in developing rat substantia nigra pars compacta dopaminergic neurones. *J Physiol* **586**, 739–750.

Burnashev N, Zhou Z, Neher E & Sakmann B (1995). Fractional calcium currents through recombinant GluR channels of the NMDA, AMPA and kainate receptor subtypes. *J Physiol* **485**, 403–418.

Cais O, Sedlacek M, Horak M, Dittert I & Vyklicky L Jr (2008). Temperature dependence of NR1/NR2B NMDA receptor channels. *Neuroscience* **151**, 428–438.

Cathala L, Brickley S, Cull-Candy S & Farrant M (2003). Maturation of EPSCs and intrinsic membrane properties enhances precision at a cerebellar synapse. *J Neurosci* **23**, 6074–6085.

Chen BS, Braud S, Badger JD 2nd, Isaac JT & Roche KW (2006). Regulation of NR1/NR2C *N*-methyl-D-aspartate (NMDA) receptors by phosphorylation. *J Biol Chem* **281**, 16583–16590.

Cik M, Chazot PL & Stevenson AF (1993). Optimal expression of cloned NMDAR1/NMDAR2A heterometic glutamate receptors: a biochemical characterization. *Biochem J* **296**, 877–883.

Cull-Candy SG & Leszkiewicz DN (2004). Role of distinct NMDA receptor subtypes at central synapses. *Sci STKE* **2004**, re16.

Dale N & Roberts A (1985). Dual-component amino-acid-mediated synaptic potentials: excitatory drive for swimming in *Xenopus* embryos. *J Physiol* **363**, 35–59.

Del Valle-Pinero AY, Suckow SK, Zhou Q, Perez FM, Verne GN & Caudle RM (2007). Expression of the *N*-methyl-D-aspartate receptor NR1 splice variants and NR2 subunit subtypes in the rat colon. *Neuroscience* **147**, 164–173.

Dravid SM, Prakash A & Traynelis SF (2008). Activation of recombinant NR1/NR2C NMDA receptors. *J Physiol* **586**, 4425–4439.

Drummond GB (2009). Reporting ethical matters in *The Journal of Physiology*: standards and advice. *J Physiol* **587**, 713–719.

Forsythe ID (1994). Direct patch recording from identified presynaptic terminals mediating glutamatergic EPSCs in the rat CNS, *in vitro*. *J Physiol* **479**, 381–387.

Forsythe ID & Barnes-Davies M (1993). The binaural auditory pathway: excitatory amino acid receptors mediate dual timecourse excitatory postsynaptic currents in the rat medial nucleus of the trapezoid body. *Proc Biol Sci* **251**, 151–157.

Forsythe ID & Westbrook GL (1988). Slow excitatory postsynaptic currents mediated by *N*-methyl-D-aspartate receptors on cultured mouse central neurones. *J Physiol* **396**, 515–533.

Futai K, Okada M, Matsuyama K & Takahashi T (2001). High-fidelity transmission acquired via a developmental decrease in NMDA receptor expression at an auditory synapse. *J Neurosci* **21**, 3342–3349.

Geiger JR, Melcher T, Koh DS, Sakmann B, Seeburg PH, Jonas P & Monyer H (1995). Relative abundance of subunit mRNAs determines gating and Ca^{2+} permeability of AMPA receptors in principal neurons and interneurons in rat CNS. *Neuron* **15**, 193–204.

Gibb AJ & Colquhoun D (1992). Activation of *N*-methyl-D-aspartate receptors by L-glutamate in cells dissociated from adult rat hippocampus. *J Physiol* **456**, 143–179.

Hardman RM & Forsythe ID (2009). *Ether-à-go-go*-related gene K^+ channels contribute to threshold excitability of mouse auditory brainstem neurons. *J Physiol* **587**, 2487–2497.

Hatton CJ & Paoletti P (2005). Modulation of triheteromeric NMDA receptors by N-terminal domain ligands. *Neuron* **46**, 261–274.

Held H (1893). Die centrale Gehorleitung. *Arch f Anat u Physiol Anat Abtheil* **17**, 201–248.

Hermida D, Elezgarai I, Puente N, Alonso V, Anabitarte N, Bilbao A, Donate-Oliver F & Grandes P (2006). Developmental increase in postsynaptic α-amino-3-hydroxy-5-methyl-4 isoxazolepropionic acid receptor compartmentalization at the calyx of Held synapse. *J Comp Neurol* **495**, 624–634.

Iijima K, Abe H, Okazawa M, Moriyoshi K & Nakanishi S (2008). Dual regulation of NR2B and NR2C expression by NMDA receptor activation in mouse cerebellar granule cell cultures. *Proc Natl Acad Sci U S A* **105**, 12010–12015.

Isaacson JS & Walmsley B (1996). Amplitude and time course of spontaneous and evoked excitatory postsynaptic currents in bushy cells of the anteroventral cochlear nucleus. *J Neurophysiol* **76**, 1566–1571.

Joshi I, Shokralla S, Titis P & Wang LY (2004). The role of AMPA receptor gating in the development of high-fidelity neurotransmission at the calyx of Held synapse. *J Neurosci* **24**, 183–196.

Joshi I & Wang LY (2002). Developmental profiles of glutamate receptors and synaptic transmission at a single synapse in the mouse auditory brainstem. *J Physiol* **540**, 861–873.

Kerchner GA & Nicoll RA (2008). Silent synapses and the emergence of a postsynaptic mechanism for LTP. *Nat Rev Neurosci* **9**, 813–825.

Klug A & Trussell LO (2006). Activation and deactivation of voltage-dependent K^+ channels during synaptically driven action potentials in the MNTB. *J Neurophysiol* **96**, 1547–1555.

Kopp-Scheinpflug C, Tolnai S, Malmierca MS & Rubsamen R (2008). The medial nucleus of the trapezoid body: comparative physiology. *Neuroscience* **154**, 160–170.

Kornau HC, Schenker LT, Kennedy MB & Seeburg PH (1995). Domain interaction between NMDA receptor subunits and the postsynaptic density protein PSD-95. *Science* **269**, 1737–1740.

Kushmerick C, Renden R & von Gersdorff H (2006). Physiological temperatures reduce the rate of vesicle pool depletion and short-term depression via an acceleration of vesicle recruitment. *J Neurosci* **26**, 1366–1377.

Lester RA, Clements JD, Westbrook GL & Jahr CE (1990). Channel kinetics determine the time course of NMDA receptor-mediated synaptic currents. *Nature* **346**, 565–567.

Lester RA, Quarum ML, Parker JD, Weber E & Jahr CE (1989). Interaction of 6-cyano-7-nitroquinoxaline-2,3-dione with the *N*-methyl-D-aspartate receptor-associated glycine binding site. *Mol Pharmacol* **5**, 565–70.

Li W, Kaczmarek LK & Perney TM (2001). Localization of two high-threshold potassium channel subunits in the rat central auditory system. *J Comp Neurol* **437**, 196–218.

Livak KJ & Schmittgen TD (2001). Analysis of relative gene expression data using real-time quantitative PCR and the $2^{-\Delta\Delta CT}$ method. *Methods* **25**, 402–408.

Mayer ML & Westbrook GL (1987). Permeation and block of *N*-methyl-D-aspartic acid receptor channels by divalent cations in mouse cultured central neurones. *J Physiol* **394**, 501–527.

Mayer ML, Westbrook GL & Guthrie PB (1984). Voltage-dependent block by Mg^{2+} of NMDA responses in spinal cord neurones. *Nature* **309**, 261–263.

Momiyama A, Feldmeyer D & Cull-Candy SG (1996). Identification of a native low-conductance NMDA channel with reduced sensitivity to Mg^{2+} in rat central neurones. *J Physiol* **494**, 479–492.

Nakagawa H, Sato K, Shiraishi Y, Kuriyama H & Altschuler RA (2000). NMDAR1 isoforms in the rat superior olivary complex and changes after unilateral cochlear ablation. *Brain Res Mol Brain Res* **77**, 246–257.

Nowak L, Bregestovski P, Ascher P, Herbet A & Prochiantz A (1984). Magnesium gates glutamate-activated channels in mouse central neurones. *Nature* **307**, 462–465.

Oertel D (1999). The role of timing in the brain stem auditory nuclei of vertebrates. *Annu Rev Physiol* **61**, 497–519.

Pal R, Agbas A, Bao X, Hui D, Leary C, Hunt J, Naniwadekar A, Michaelis ML, Kumar KN & Michaelis EK (2003). Selective dendrite-targeting of mRNAs of NR1 splice variants without exon 5: identification of a cis-acting sequence and isolation of sequence-binding proteins. *Brain Res* **994**, 1–18.

Popescu G & Auerbach A (2003). Modal gating of NMDA receptors and the shape of their synaptic response. *Nat Neurosci* **6**, 476–483.

Postlethwaite M, Hennig MH, Steinert JR, Graham BP & Forsythe ID (2007). Acceleration of AMPA receptor kinetics underlies temperature-dependent changes in synaptic strength at the rat calyx of Held. *J Physiol* **579**, 69–84.

Rumbaugh G, Prybylowski K, Wang JF & Vicini S (2000). Exon 5 and spermine regulate deactivation of NMDA receptor subtypes. *J Neurophysiol* **83**, 1300–1306.

Samson AL, Nevin ST, Croucher D, Niego B, Daniel PB, Weiss TW, Moreno E, Monard D, Lawrence DA & Medcalf RL (2008). Tissue-type plasminogen activator requires a co-receptor to enhance NMDA receptor function. *J Neurochem* **107**, 1091–1101.

Sato K, Nakagawa H, Kuriyama H & Altschuler RA (1999). Differential distribution of *N*-methyl-D-aspartate receptor-2 subunit messenger RNA in the rat superior olivary complex. *Neuroscience* **89**, 839–853.

Schneggenburger R & Forsythe ID (2006). The calyx of Held. *Cell Tissue Res* **326**, 311–337.

Song P, Yang Y, Barnes-Davies M, Bhattacharjee A, Hamann M, Forsythe ID, Oliver DL & Kaczmarek LK (2005). Acoustic environment determines phosphorylation state of the Kv3.1 potassium channel in auditory neurons. *Nat Neurosci* **8**, 1335–1342.

Spruston N, Jonas P & Sakmann B (1995). Dendritic glutamate receptor channels in rat hippocampal CA3 and CA1 pyramidal neurons. *J Physiol* **482**, 325–352.

Steinert JR, Kopp-Scheinpflug C, Baker C, Challiss RA, Mistry R, Haustein MD, Griffin SJ, Tong H, Graham BP & Forsythe ID (2008). Nitric oxide is a volume transmitter regulating postsynaptic excitability at a glutamatergic synapse. *Neuron* **60**, 642–656.

Taschenberger H & von Gersdorff H (2000). Fine-tuning an auditory synapse for speed and fidelity: developmental changes in presynaptic waveform, EPSC kinetics, and synaptic plasticity. *J Neurosci* **20**, 9162–9173.

Tovar KR, Sprouffske K & Westbrook GL (2000). Fast NMDA receptor-mediated synaptic currents in neurons from mice lacking the ε2 (NR2B) subunit. *J Neurophysiol* **83**, 616–620.

Traynelis SF, Burgess MF, Zheng F, Lyuboslavsky P & Powers JL (1998). Control of voltage-independent zinc inhibition of NMDA receptors by the NR1 subunit. *J Neurosci* **18**, 6163–6175.

von Gersdorff H & Borst JG (2002). Short-term plasticity at the calyx of Held. *Nat Rev Neurosci* **3**, 53–64.

Wong AY, Graham BP, Billups B & Forsythe ID (2003). Distinguishing between presynaptic and postsynaptic mechanisms of short-term depression during action potential trains. *J Neurosci* **23**, 4868–4877.

Woodhull AM (1973). Ionic blockage of sodium channels in nerve. *J Gen Physiol* **61**, 687–708.

Yuan H, Vance KM, Junge CE, Geballe MT, Snyder JP, Hepler JR, Yepes M, Low CM & Traynelis SF (2009). The serine protease plasmin cleaves the amino-terminal domain of the NR2A subunit to relieve zinc inhibition of the *N*-methyl-D-aspartate receptors. *J Biol Chem*.

Zhang S & Trussell LO (1994). Voltage clamp analysis of excitatory synaptic transmission in the avian nucleus magnocellularis. *J Physiol* **480**, 123–136.

Author contributions

The project was initiated by M.P. (persistence of NMDAR in mature rats at physiological temperature) and I.D.F., then continued and extended by M.D.J. and J.R.S. The work was conducted under the supervision of I.D.F. and the manuscript was written by I.D.F. with input from all authors, but especially J.R.S. Experimental work was conducted initially in the Department of Cell Physiology and Pharmacology and then the MRC Toxicology Unit, University of Leicester.

Acknowledgements

This research was funded by the MRC and BBSRC. Thanks to Paul Chazot for the kind gift of antibodies to NR2A, and to Robert Pawlak for access to tissue from the tPA knockout mouse.

Authors' present addresses

M. Postlethwaite: GU Biology, Pfizer Global R&D, Ramsgate Road, Sandwich CT13 9NJ, UK.